JGR Oceans

RESEARCH ARTICLE
10.1029/2021JC017774

Sensitivity of Sea-Surface Enthalpy and Momentum Fluxes to Sea Spray Microphysics

Sydney Sroka[1] **and Kerry Emanuel**[1]

[1]Lorenz Center, Massachusetts Institute of Technology, Cambridge, MA, USA

Key Points:

- In high winds, most of the spray will reenter the sea close to the wet-bulb temperature, the free stream wind speed, and the initial size
- The ratio of the enthalpy and momentum exchange coefficients is likely independent of wind speed beyond a threshold wind speed
- In high wind speeds, the spray mass flux appears to be more important than the drop size distribution for the spray-mediated fluxes

Correspondence to:
S. Sroka,
ssroka@mit.edu

Citation:
Sroka, S., & Emanuel, K. (2022). Sensitivity of sea-surface enthalpy and momentum fluxes to sea spray microphysics. *Journal of Geophysical Research: Oceans*, *127*, e2021JC017774. https://doi.org/10.1029/2021JC017774

Received 11 JUL 2021
Accepted 7 DEC 2021

Abstract Accurate estimates of air-sea enthalpy and momentum fluxes are critically important for hurricane intensity predictions. However, calculating these fluxes is challenging due to the nature of the air-sea transition region. At extreme wind speeds, a substantial amount of sea spray is lofted making it necessary to calculate the sea spray-mediated enthalpy and momentum fluxes. These calculations rely on microphysical equations, which are sensitive to the details of the local environmental conditions. Here we use a microphysical model to show that there exists a threshold wind speed beyond which the net sea spray-mediated enthalpy and momentum fluxes are well-approximated by using the net sea spray mass flux alone. This result supports the hypothesis that at extreme wind speeds, the ratio of the air-sea exchange coefficients becomes independent of wind speed, implying the air-sea flux calculations can be substantially simplified.

Plain Language Summary A hurricane's intensity is very sensitive to the energy exchange processes at the sea surface, and so it is important for models to have accurate air-sea interaction schemes. At extreme wind speeds, the rates at which the air and sea exchange enthalpy and momentum are different from those of calm conditions and calculating the air-sea exchange is complicated by the microphysics of evaporating sea spray. In this regime, sea spray is ubiquitous and there is no well-defined air-sea interface. We use a microphysical model to show that once the wind speed is high enough, the air-sea exchange calculation can be substantially simplified and the fluxes primarily depend on the total volume of sea spray.

1. Introduction

The air-sea fluxes of enthalpy and momentum are the governing thermal energy source and mechanical energy sink, which control hurricane intensity, but representing these fluxes in simulations is challenging. Many models employ bulk parameterizations of air-sea fluxes that often exhibit a significant sensitivity between the simulated hurricane intensity and the bulk exchange coefficients for enthalpy (C_K) and momentum (C_D) (Green & Zhang, 2014; Ma et al., 2017; Nystrom et al., 2020; Torn, 2016). The ratio of these coefficients C_K/C_D is especially important for modeling hurricanes, since it is directly proportional to several key intensity metrics, including the square of the maximum potential intensity (Emanuel, 1986, 1995). While there have been a few studies that used direct measurements from GPS dropsondes, ocean buoys, and/or airborne radar to measure surface fluxes at high wind speeds (Black et al., 2007; Holthuijsen et al., 2012; Powell et al., 2003; Richter & Stern, 2014; Zou et al., 2018), the sparsity of direct observations makes model verification challenging. Additionally, the nature of the near-surface region at high wind speeds presents substantial challenges that inhibit surface flux calculations since the air-sea interface is no longer well-defined due to the presence of sea spray, bubbles, and foam (Emanuel, 2003; Holthuijsen et al., 2012; Sroka & Emanuel, 2021). Theoretical models, laboratory experiments, and numerical simulations have shown that the microphysical processes that govern sea spray generation, evaporation, and acceleration can have a significant effect on the large-scale air-sea exchange of enthalpy and momentum (Andreas & Emanuel, 2001; Jeong et al., 2012; Mueller & Veron, 2014a, 2014b; Peng & Richter, 2017, 2019, 2020; Troitskaya, Druzhinin, et al., 2018; Troitskaya, Kandaurov, et al., 2018).

The amount of sea spray-mediated enthalpy and momentum flux is determined by: (a) the local meteorological conditions in the spray layer, (b) the amount of time a drop remains aloft, and (c) the sea spray generation function (SSGF). The microphysical model used in this study to calculate how drops evaporate and accelerate in response to the local conditions for a given residence time parameterization is described throughout Andreas (1989, 1990, 1992, 1995) and Andreas (2004) and is discussed in detail in Section 3. This model has been used to estimate sea spray fluxes in both small-scale Lagrangian particle simulations (Druzhinin et al., 2018; Peng & Richter, 2017, 2019, 2020) and large-scale numerical simulations of hurricanes (Garg et al., 2018). According to

this model, the sea spray-mediated enthalpy flux is primarily a function of the relative humidity, the air-sea temperature difference, and the sea surface temperature, while the sea spray-mediated momentum flux is primarily a function of the surface wind speed (Andreas, 2004; Andreas & Emanuel, 2001). Since spray drops will undergo more evaporation and accelerate to faster speeds, the longer they remain aloft a residence time formulation is needed. The primary formulation used by this study is from Andreas (1992). Many SSGFs, which describe the rate at which drops of different sizes are ejected, for the open ocean have come from the sea spray aerosol community as reviewed in Lewis et al. (2004), O'Dowd and De Leeuw (2007), and De Leeuw et al. (2011), though these tend to primarily consider small drops with radii less than approximately 10 μm. The present analysis is focused on larger drops with radii ranging from approximately 50–2,000 μm. Sea spray generation functions that primarily consider these larger drop sizes are reviewed in Andreas (2002) and Veron (2015), but relatively few of these were developed from observations in the field or laboratory in the high wind regime. The functions considered in this analysis were all developed using high wind speed observations to reduce the extent to which extrapolation errors affect the estimated sea spray production rate.

The SSGF is likely the largest source of uncertainty in the sea spray-mediated flux calculation. While the total volume flux predicted by the SSGF and the way it changes with wind speed are essential for estimating the sea spray fluxes, the results from this analysis suggest that the drop size distribution may not be as critical. While a drop's mass does affect how much enthalpy and momentum it can mediate, if the majority of the total volume of sea spray undergoes the same temperature and velocity changes, then the spray fluxes can be estimated without the drop size distribution.

2. A Mechanistic Argument

Emanuel (2003), hereafter E3, presented a mechanistic argument based on an idealized setup and a few simplifying assumptions. Specifically, he assumed that at very high wind speeds, such that all the momentum and heat fluxes are carried by spray,

1. newly ejected, upward traveling drops are at the sea surface temperature T_s and have negligible horizontal velocity, while reentrant, downward traveling drops are at the far-field wet-bulb temperature T_w and have a mass-weighted average horizontal velocity u_{sp},
2. the net evaporation is a small fraction of the total lofted mass of sea spray; thus, the net downward spray mass flux is nearly equal to its upward flux.

The assumption that the sea spray carries all of the momentum and heat fluxes is crucial for this model, but the true distribution between sea spray fluxes and interfacial fluxes in the high wind speed limit is uncertain. While the findings from several studies suggest that sea spray carries at least the majority, if not all, of the air-sea heat flux at extreme wind speeds (Mueller & Veron, 2014a; Richter & Stern, 2014; Troitskaya, Druzhinin, et al., 2018), there is more disagreement surrounding the momentum flux. While the theoretical study of Andreas (2004) suggests that sea spray can support the full air-sea momentum flux at 10-m wind speeds above 60 m/s, albeit with the acknowledgment that this behavior at high wind speeds is "very speculative," other studies attribute most of the momentum flux to the wave form drag. Estimating the wave form drag at extreme wind speeds is very challenging without definitive observations. One technique to do so involves extrapolating results from lower wind speed observations into the high wind speed regime (Troitskaya, Druzhinin, et al., 2018), but this method may overestimate the form drag. At lower wind speeds, there is less spray and the waves likely have steeper slopes than they do at extreme wind speeds where there is some evidence that the wave slopes are suppressed by the copious wave-breaking (Komori et al., 2018). Other estimates that include significant contributions from wave form drag come from Lagrangian particle simulations where the shape of the surface and number of injected particles are prescribed (Richter et al., 2019) or from models in which sea spray is assumed to be primarily confined to a very narrow slip layer above the surface (Makin, 2005).

If the aforementioned assumptions are satisfied, then the net surface stress and upward enthalpy flux are given by

$$\tau = M_u u_{sp} \tag{1}$$

and

$$F = M_u c_l (T_s - T_w), \tag{2}$$

where M_u is the upward flux of spray mass per unit area, c_l is the heat capacity of liquid water, T_s is the ocean temperature, and T_w is the ambient wet-bulb temperature. If we were to represent these fluxes with conventional aerodynamic flux formulae, they would be, respectively,

$$\tau = C_{Dh} \rho_a u_h^2 \tag{3}$$

and

$$F = C_{kh} \rho_a u_h (k_0^* - k_h) \tag{4}$$

where C_{Dh} is a drag coefficient defined at altitude h, C_{kh} is an enthalpy flux coefficient also defined at altitude h, ρ_a is the air density, u_h is the wind speed at altitude h, k_0^* is the saturation moist enthalpy of the sea surface, and k_h is the moist enthalpy at altitude h.

If we now substitute the spray-related stress and enthalpy flux Equations 1 and 2 into Equations 3 and 4, we get

$$\frac{C_{kh}}{C_{Dh}} = \frac{u_h}{u_{sp}} \frac{c_l (T_s - T_w)}{k_0^* - k_h}. \tag{5}$$

E3 chose the height h rather than being a fixed altitude to always be the altitude at which the air velocity equals the spray speed u_{sp} and further assumed that the latter is always some constant fraction of the gradient wind speed u_g. If this last assumption is satisfied, then the ratio of exchange coefficients that should be applied to the gradient wind is

$$\frac{C_{kg}}{C_{Dg}} = \frac{c_l (T_s - T_w)}{k_0^* - k_h}, \tag{6}$$

where C_{kg} and C_{Dg} are, respectively, the exchange coefficients for enthalpy and momentum applicable to the gradient wind. E3 showed that if $T_s - T_w$ is a small fraction of the absolute temperature, such that the Clausius-Clapeyron equation can be linearized, Equation 6 can be simplified to

$$\frac{C_{kg}}{C_{Dg}} = \frac{c_l}{c_p + \frac{L_v^2 q_a}{R_v T_a^2}}, \tag{7}$$

where c_p is the heat capacity at constant pressure for air, L_v is the latent heat of vapourization, q_a^* is the saturation-specific humidity at the air temperature, R_v is the gas constant for water vapor, and T_a is the air temperature. Owing to the strong dependence of q_a^* on temperature, the ratio of exchange coefficients given by Equation 7 is a decreasing function of air temperature (as shown in Figure 3 of Emanuel, 2003), but it is not a function of wind speed.

Again, the assumptions from E3 are based on the limiting case in which all of the momentum and heat flux are carried by sea spray. An implication of these assumptions is that the fractions of the thermal and wind speed environmental variables that sea spray drops attain are the same (i.e., $T/T_w = u/U_{10}$ where T and u are the temperature and speed of the sea spray drops, respectively) and invariant with u_*. This implies that the ratio C_K/C_D also does not vary with u_*.

The aim of this study is to use the microphysical model to evaluate if and when the main assumptions of the mechanistic argument are met and to estimate the threshold wind speed beyond which the ratio of the exchange coefficients is expected to become independent of wind speed. The microphysical model and the SSGFs used to calculate the sea spray-mediated enthalpy and momentum fluxes are described in Sections 3 and 4, respectively. Section 5 analyzes an ensemble of drop evaporation time histories to evaluate if and when the assumptions from the mechanistic argument are met. Finally, Section 6 summarizes the results.

3. The Microphysical Model

3.1. The Momentum Flux

The sea spray-mediated momentum flux is computed according to the model presented in Andreas (2004). Drops are assumed to be accelerated from rest by a uniform wind field with a velocity equal to the 10-m wind speed U_{10}. The time tendency of the speed of a drop u is given by

$$\frac{du}{dt} = \frac{3}{8} C_d(\mathrm{Re}) \frac{\rho_a}{\rho_l} \frac{(U_{10} - u)^2}{r_0} \tag{8}$$

where ρ_l is the density of sea water and r_0 is the initial drop radius. The drag coefficient for a spherical drop $C_d(\mathrm{Re})$ is a function of the Reynolds number Re, which is defined as $Re = (U_{10} - u)(2r_0)/\nu_a$ where ν_a is the kinematic viscosity of air. Following Andreas (2004), the drag formulation used here is from Clift et al. (1978). The spray stress from one drop is then $m_0 u$, where m_0 is the initial mass and u is the horizontal speed the drop attains before returning to the sea. This model technically represents an upper bound on the momentum flux since it neglects evaporation. However, as will be shown in Section 5, the total evaporated mass is expected to be a very small fraction of the total ejected mass.

3.2. The Enthalpy Flux

The cloud microphysics evaporation equations from Pruppacher and Klett (1978) formed the basis for the sea spray evaporation model developed throughout Andreas (1989, 1990, 1992, 1995). The coupled system of equations, which describes the evolution of the temperature T and radius r of a saline drop, using the symbolism from Andreas (2005), is

$$\frac{\partial T}{\partial t} = \frac{3\left(k_a'(T_a - T) + L_v D_w'(\rho_v - \rho_{v,r})\right)}{\rho_l c_l r^2} \tag{9}$$

$$\frac{\partial r}{\partial t} = \frac{\left[\left(\frac{RH}{100} - 1\right) - y\right] r^{-1}}{\frac{\rho_l R T_a}{D_w' M_w e_{\mathrm{sat}}(T_a)} + \frac{\rho_l L_v}{k_a' T_a}\left(\frac{L_v M_w}{R T_a} - 1\right)} \tag{10}$$

where k_a' is the thermal conductivity modified for noncontinuum behavior, D_w' is the vapor diffusivity modified for noncontinuum behavior, ρ_v is the ambient vapor density, $\rho_{v,r}$ is the vapor density at the drop's surface, RH is the percent relative humidity, y is the curvature parameter, R is the universal gas constant, M_w is the molar mass of water, and e_{sat} is the saturated partial pressure of water vapor. For this study, the sea water parameters L_v, ρ_l, and c_l are functions of temperature and salinity according to Nayar et al. (2016), the ambient pressure is assumed to be 1,000 mb, and the salinity of sea water is assumed to be 34 ppt. With these assumptions, there are only three external parameters that define the time tendency of evaporation for a drop: the relative humidity RH, the air-sea temperature difference $\Delta T = T_s - T_a$, and the sea surface temperature T_s.

Andreas and Emanuel (2001) described how a drop will quickly cool to T_w after ejection, generally losing less than 1% of its mass in the process. The characteristic timescale for this thermal adjustment is τ_T, which is the time it takes for a drop's temperature to come within an e-folding fraction of its wet-bulb temperature (Andreas, 1992). After a drop has reached its wet-bulb temperature, it exchanges sensible for latent heat with the atmosphere and loses mass until it has warmed to T_a and has evaporated to its equilibrium radius r_{eq}. The mass loss timescale for a drop is τ_r, which is the time it takes for a drop's radius to come within an e-folding fraction of its equilibrium radius (Andreas, 1992). Andreas and Emanuel (2001) demonstrated that the two processes of cooling to T_w and completely evaporating to a radius of r_{eq} are essentially temporally decoupled; in other words, $\tau_T \ll \tau_r$.

In this model, drops are assumed to be initially at the sea surface temperature, to experience uniform ambient air conditions until they reenter the sea after a time τ_f and to not interact with other drops, which gives an upper bound on the enthalpy flux. Using the symbolism from Troitskaya, Druzhinin, et al. (2018), the enthalpy flux from a drop is calculated as

$$Q = c_l(m_0 T_s - m_f T(\tau_f) - (m_0 - m_f) T_a) \tag{11}$$

where m_f is the drop's mass at reentrance. Several studies including Mueller and Veron (2014b) and Peng and Richter (2019) suggested that these assumptions overestimate the total sea spray-mediated flux due to smaller drops rapidly condensing and warming right before reentrance as they approach the sea even if they were able to thermally adjust to nearly their wet-bulb temperature at some point during their flight. Peng and Richter (2020) used Lagrangian particle simulations to look for interactions between drops of different sizes and found that large drops are more heavily concentrated near the bottom of the spray layer and can increase the moist enthalpy of the lower region to further reduce the net enthalpy contribution of small drops. Fairall et al. (2009) found that the slope of the waves played an important role in determining whether large drops would spend a significant time aloft. Mueller and Veron (2014b), Richter et al. (2019), and Peng and Richter (2020) all raised the concern that large drops may not be transported high enough to experience ambient conditions of T_a, RH, or U_{10} during their flight. One consideration is that most of these studies, with the exception of Mueller and Veron (2014b) who simulated 10-m wind speeds as high as 50 m/s, generally reported results for 10-m wind speeds below the high wind speeds that are primarily of interest in this study; at lower wind speeds, less sea spray is expected to be produced and the ejected spray is not expected to be lofted as high or remain aloft for as long. However, incorporating these interactions could change the threshold wind speed at which the mechanistic argument assumptions are satisfied but would not change the conclusions about the high wind speed limit.

This analysis also assumes that there are no spray-feedback effects on the external environmental parameters. The feedback model from Andreas et al. (2015) considered the sea spray-mediated enthalpy flux as part of a positive feedback loop that helped extract more enthalpy from the sea surface, while the results from the Lagrangian simulation from Peng and Richter (2019) found that sea spray-mediated enthalpy flux modulated the near-surface region as part of a negative feedback loop, which suppressed the enthalpy flux from the sea surface. While feedback effects are likely to change the amount of sea spray-mediated flux, they are less likely to affect the fundamental dependencies between T_s, T_w, and U_{10}. Moreover, if the vertical profiles of enthalpy and momentum in the spray layer obey the same law (e.g., a logarithmic dependence on z), then spray feedbacks should not affect the ratio of the exchange coefficients.

Following the format of the figures from Andreas (1995) and Andreas and Emanuel (2001), Figure 1 illustrates how the three external parameters (RH, ΔT, and T_s) and the initial radius r_0 affect the temperature and radius evolution of an evaporating drop. As shown in Figure 1a, increasing the relative humidity has two opposing effects. The first is that a higher RH leads to a higher T_w, which decreases the enthalpy flux potential. The second effect is that a higher RH suppresses evaporative mass loss, which increases the enthalpy flux potential primarily for drops that remain aloft longer than τ_r. Figures 1b and 1c show that changing ΔT or T_s has a negligible effect on the drop's mass loss rate, but does affect the enthalpy flux potential. A larger ΔT at the same T_s lowers the wet-bulb temperature, increasing the enthalpy flux potential. Increasing T_s for the same ΔT does slightly increase the enthalpy flux potential (see Figure 1c annotations) through the temperature dependence of the saturation-specific humidity. Finally, Figure 1d shows that drops of different sizes will evaporate at different rates; larger drops take longer to reach both T_w and r_{eq}, but transfer more enthalpy in the process.

3.3. The Residence Time

Andreas and Emanuel (2001) demonstrated that a significant enhancement to the air-sea enthalpy flux in hurricanes could come from reentrant spray, which are spray drops that reenter the sea after partially evaporating. The residence time proposed by Andreas (1992) is

$$\tau_f = \frac{A_s}{u_f} \tag{12}$$

where A_s is the significant wave amplitude and u_f is the Stokes fall speed modified for large Reynolds numbers and large drops as defined in Andreas (1989, 1990) and based on Batchelor (1970) and Friedlander (1977). This parameterization considers drops to remain aloft for as long as it takes them to fall a distance A_s through still air. The findings from several numerical simulation studies of the drop spray layer, including Andreas et al. (1995), Edson et al. (1996), and Van Eijk et al. (2001), support the use of A_s as characteristic length scale for the residence time. Turbulence-enhanced residence times are indirectly parameterized through the significant wave amplitude A_s. Andreas (1992) uses the parameterization $A_s = 0.015\, U_{10}^2$ following the results from Kinsman (1965); Wilson (1965) and Earle (1979); note that the coefficient 0.015 effectively has the units of s^2/m for U_{10} with units of

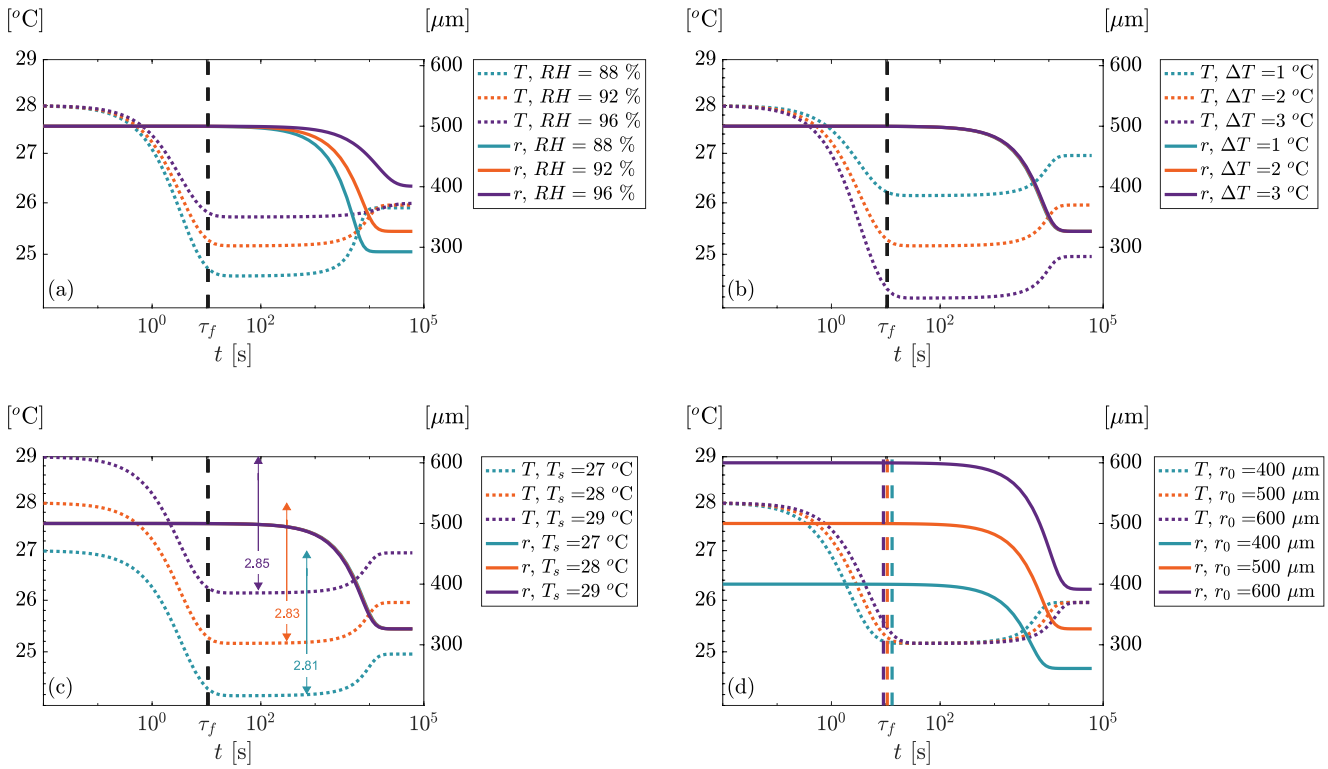

Figure 1. These results show how the evaporation is affected by changes in the relative humidity (a), air-sea temperature difference (b), sea surface temperature (c), and initial drop radius (d). All other parameters are held constant at their default values ($RH = 92\%$, $\Delta T = 2°C$, $T_s = 28°C$, and $r_0 = 500\ \mu m$). The residence time τ_f is calculated for $U_{10} = 54$ m/s. Note that neither changes in the air-sea temperature difference nor in the sea surface temperature have much effect on the rate at which the drop's radius decreases.

m/s. Figure 1d shows how the τ_f decreases as the initial radius of the drop and therefore, the modified Stokes fall speed increases.

Some Lagrangian particle simulations found a much weaker dependence of τ_f on U_{10} or did not find a clear relationship between τ_f and A_s (Mestayer et al., 1996; Mueller & Veron, 2014b). However, as discussed in Troitskaya, Druzhinin, et al. (2018), one of the problematic aspects of Lagrangian particle simulations is their choice of initial velocities for the spray particles to which the residence time is very sensitive. While imperfect, τ_f from Andreas (1992) is a good heuristic for the goals of this analysis. Additionally, as will be discussed later, the results of this analysis are robust to a few variations of the residence time formulation.

Figure 2 compares the four characteristic timescales τ_r, τ_T, τ_f, and τ_{ac} for a sample of drops; these plots are similar to the curves shown in Figure 1 of Andreas (1992) and Figure 1 of Andreas (2004), except here the 10-m wind speed is the independent variable to emphasize the wind speed dependence of τ_f and τ_{ac}. For comparison, the contours of τ_f and τ_{ac} for the other drop sizes are plotted in gray.

By examining the curves in Figure 2, it is possible to approximately bound the drop sizes, which are expected to mediate the maximum amount of enthalpy and momentum for their size. Drops with initial radii less than approximately $r_0 = 500\ \mu m$ have a residence time τ_f that is greater than τ_T for U_{10} above 30 m/s. Therefore, drops in this range can be expected to reach their wet-bulb temperature. However, drops smaller than approximately $r_0 = 100\ \mu m$ are expected to lose a substantial amount of their mass and warm to nearly T_a since at high wind speeds, their residence time is expected to exceed τ_r. Drops much larger than $r_0 = 500\ \mu m$ may not have sufficient time aloft to cool to T_w before reentering since for very large drops, τ_f is much less than τ_T. Since the amount of enthalpy a drop can mediate scales with r_0^3, larger drops can mediate much more enthalpy than smaller drops. Therefore, even if larger drops do not transfer the maximum amount of enthalpy by reentering at T_w, they can still account for a substantial contribution to the net enthalpy flux.

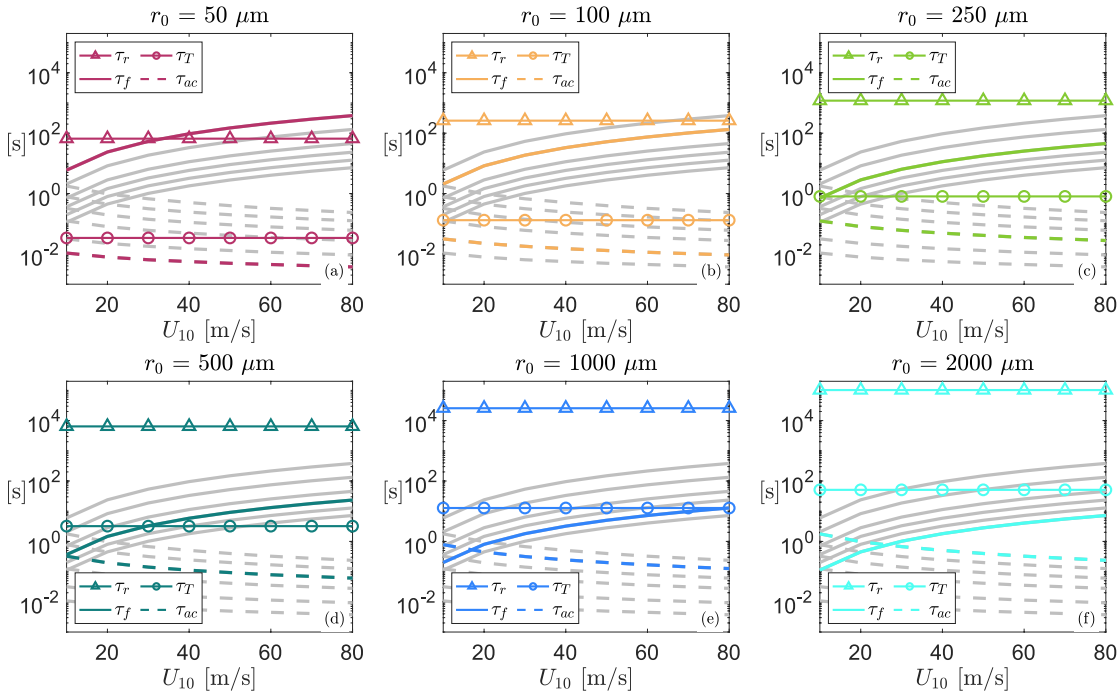

Figure 2. The curves plotted in color denote the four timescales relevant for the enthalpy and momentum transfer potential of a drop: τ_r (mass loss timescale), τ_T (thermal adjustment timescale), τ_f (residence time), and τ_{ac} (acceleration timescale). Note that τ_r and τ_T are independent of U_{10}. For comparison, the τ_f and τ_{ac} curves for the other drop sizes are plotted in gray. The environmental variables used here match the default values from Figure 1.

Since a drop extracts more momentum as it accelerates to higher speeds, it is important to compare a drop's residence time to its acceleration timescale τ_{ac}, which is when the drop's velocity is within an e-folding fraction of U_{10} (Andreas, 2004). Figure 2, like figure 1 of Andreas (2004), shows how τ_{ac} compares to τ_f for different drop sizes. For $U_{10} > 30$ m/s, even the largest drops will have accelerated to nearly U_{10}. The Weber number, defined as $\rho_a U_{10}^2 r_0/\sigma$, where σ is the surface tension, compares inertial forces to surface tension forces. The Weber number far exceeds the critical value of 6 (Villermaux & Bossa, 2009) for the case of a 2,000 μm drop moving at 30 m/s. This suggests that the drop would breakup if it did not reenter the sea first. However, drop breakup would only produce smaller drops that would be accelerated more quickly. Since each figure shows $\tau_f > \tau_{ac}$ for $U_{10} > 30$ m/s, all drops in the range considered here are expected to mediate the maximum amount of momentum.

4. Sea Spray Generation Functions

The three SSGFs considered in this study are shown in Figure 3 and were developed using observations from high wind speed conditions. A SSGF, denoted $\frac{dF}{dr_0}$, defines the number of drops produced per square meter, per second, per increment drop radius. Zhao et al. (2006) developed a SSGF by curve fitting observations of sea spray volume flux from field and laboratory experiments. The authors considered the volume flux to be a function of the dimensionless windsea Reynolds number, which depends on both the wind speed and the development of the sea surface (Toba et al., 2006). The windsea Reynolds number is defined as $Re_B = C_D U_{10}^2/(\omega_p \nu_a)$, where C_D is the sea surface drag and ω_p is the peak spectral frequency of the surface wave field. Using Re_B rather than a wind speed variable was advantageous in other air-sea exchange studies (Iida et al., 1992; Toba & Koga, 1986; Toba et al., 2006; Zhao & Toba, 2001; Zhao et al., 2003) and is especially helpful when analyzing data from both laboratory and field experiments since the differences in fetch are accounted for through ω_p, although ω_p is not truly an external parameter. The data spanned 10-m wind speeds from 8 m/s to 41 m/s and Re_B from 2,000 to 30,000. Since the observations were collected at different sea surface-relative heights, the authors used the methodology from Slinn and Slinn (1980) and Fairall and Larsen (1984) to estimate the flux at the sea surface. The curve fit of the volume flux was combined with the drop size distribution from Monahan (1968) to arrive at their final SSGF. As shown in Figure 3b, their SSGF (Equation 17 in their paper) predicts that drops with r_0 between 75 and 200 μm make up the largest share of the total spray volume flux.

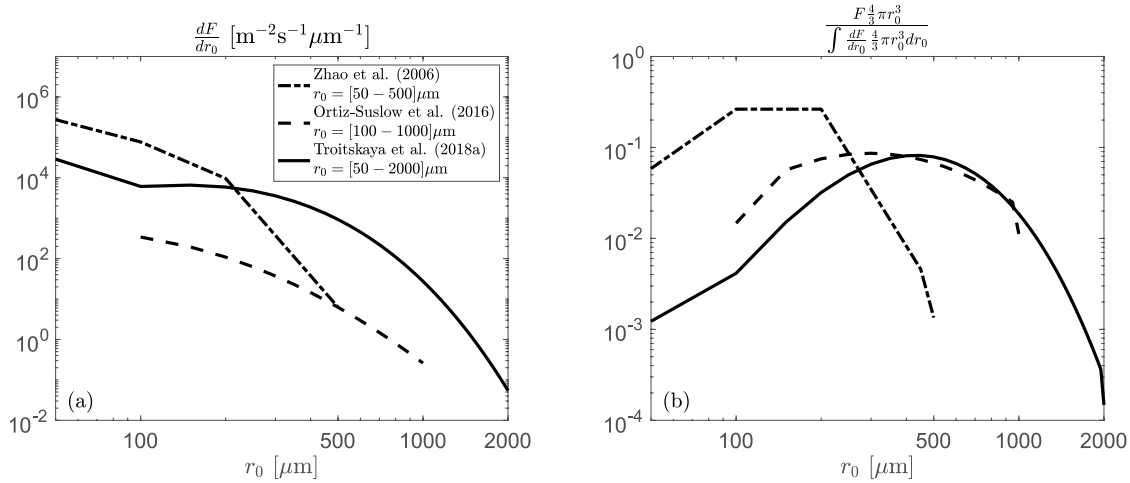

Figure 3. These plots show the three sea spray generation functions from Zhao et al. (2006), Ortiz-Suslow et al. (2016), and Troitskaya, Kandaurov, et al. (2018) (a) and the normalized volume flux from each function (b). All of the functions are evaluated at $U_{10} = 54$ m/s, and the functions from Zhao et al. (2006) and Troitskaya, Kandaurov, et al. (2018) are evaluated at a wave age of $\beta = 0.4$.

Ortiz-Suslow et al. (2016) conducted wave tank experiments at high wind speeds and observed the drop spectrum that was generated. The experiments tested equivalent 10-m wind speeds from 36 m/s to 54 m/s and the authors, namely Zhao et al. (2006), also used curve fitting to create an SSGF (here, we use the fitted relation in Equation 22 in their paper rather than their empirical formulation). There are a couple of possible reasons this function exhibits a much lower flux than the other wave tank experiment considered in this study by Troitskaya, Kandaurov, et al. (2018). The first simply has to do with differences in the experimental setups, including the tank dimensions, the salinity of the water, and the height at which drops were observed. Ortiz-Suslow et al. (2016) observed drops at $2.5H_s$, where H_s is the significant wave height, and then calculated the equivalent spray generation at H_s compared to Troitskaya, Kandaurov, et al. (2018) who observed drop production at the surface. A second possible explanation has to do with how the equivalent profile at H_s was calculated. As explained in both Ortiz-Suslow et al. (2016) and Mehta et al. (2019), the profile transformation relies on a standard, albeit imperfect, parameterization of the drop deposition velocity. This experiment still observed many more large drops than previous, lower wind speed experiments and helps this analysis consider the possibility that drops need to rise above H_s to begin evaporating. Their SSGF predicts that drops with r_0 between approximately 200 and 400 μm make up the largest share of the total spray volume flux.

The results from the wave tank experiments conducted by Troitskaya, Kandaurov, et al. (2018) demonstrated why it is critical to consider SSGFs created from high wind speed observations rather than functions that were extrapolated from low wind speed observations into the high wind speed regime. The authors tested a range of equivalent 10-m wind speeds from 18 m/s to 33 m/s and found that the dominant the sea spray creation mechanism at high wind speeds, known as bag-breakup (Veron et al., 2012), both significantly changed the sea spray drop size distribution and was only activated beyond a certain threshold wind speed. In their setup, this generation mechanism, which leads to the production of many more large drops, became the dominant mechanism of sea spray production above an equivalent U_{10} of about 24 m/s and a windsea Reynolds number of 8,000. The authors note that in open ocean conditions where the fetch is not limited, this threshold wind speed would likely be lower. As previously noted, unlike Ortiz-Suslow et al. (2016), spray production in these experiments was observed at the water surface. Their SSGF (Equation 24 in their paper) predicts that drops with r_0 between approximately 400 and 500 μm make up the largest share of the total spray volume flux.

Many studies write the windsea Reynolds number in terms of the wave age parameter $\beta = g/(\omega_p U_{10})$ such that $Re_B = C_D U_{10}^3 \beta/(g\nu_a)$, where g is gravity. The SSGFs from Zhao et al. (2006) and Troitskaya, Kandaurov, et al. (2018) are both proportional to $\beta^{1.5}$ since Troitskaya, Kandaurov, et al. (2018) followed Zhao et al. (2006) during the part of their derivation. The SSGF from Ortiz-Suslow et al. (2016) does not extrapolate the sea spray flux based on a wave state parameter like the wave age or the windsea Reynolds number since it was developed from direct observations of sea spray at a fixed height. Typical field conditions have a wave age of $\beta = 0.4$, so this

Table 1
The 8400-Member Ensemble of Drop Evaporation Time Histories Comprised Permutations of the Three Independent Parameters T_s, ΔT, and RH Evaluated at Each Drop Radius From 50 to 2,000 μm Using 50 μm Increments

	Units	Range	Increment
T_s	[°C]	[27, 29]	1
ΔT	[°C]	[0.5, 3.5]	0.5
RH	[%]	[80, 98]	2
r_0	[μm]	[50, 2,000]	50

value is used in both SSGFs from Zhao et al. (2006) and Troitskaya, Kandaurov, et al. (2018), but the proportionality of the spray volume flux to β is such that the three normalized ratios in Section 5 are insensitive to the choice of β.

5. Results

The assumptions evaluated in this section, whether the majority of the sea spray volume reenters the sea at nearly T_w, whether the evaporated volume of sea spray is a small fraction of the total lofted volume, and whether the majority of the sea spray volume is moving at nearly the free stream wind speed before reentrance, were found to be true for a drop with $r_0 = 100$ μm under typical hurricane spray layer conditions ($T_s = 28$°C, $\Delta T = 1$°C, and $RH = 80\%$) in Andreas and Emanuel (2001). The present analysis evaluates a wider range of conditions and drop sizes to explore the sensitivity of the sea spray-mediated fluxes to the size distributions of the three aforementioned SSGFs.

In the following three sections, we evaluate the three main assumptions in the mechanistic argument using an ensemble of 8,400 integrations of Equations 9 and 10 corresponding to each permutation of the set of RH, ΔT, T_s, and r_0 listed in Table 1. This range of r_0 was chosen because drops smaller than 50 μm are not expected to contribute much to the net spray fluxes under high wind speeds, and none of the SSGFs are valid for drop sizes larger than 2,000 μm. Each SSGF is only evaluated for the range of drop sizes within this set for which the SSGF is valid; the Zhao et al. (2006) SSGF is evaluated for initial radii $r_0 \in [50-500]$ μm, the Ortiz-Suslow et al. (2016) SSGF is evaluated for initial radii $r_0 \in [100-1{,}000]$ μm, and the Troitskaya, Kandaurov, et al. (2018) SSGF is evaluated for initial radii $r_0 \in [50-2{,}000]$ μm. The circles in Figure 4 indicate the mean value of the ensemble at the corresponding wind speed and the whiskers represent one standard deviation from the mean.

5.1. Spray Drops Reenter at a Temperature of Nearly T_w

The temperature time histories from the ensemble showed that most of the sea spray mass is expected to reenter the sea very close to the wet-bulb temperature. Figure 4a shows γ_1, which compares the amount a drop cools between ejection and reentrance ($T_s - T(\tau_f)$) to the maximum potential cooling ($T_s - T_w$) weighted by the total sea spray volume flux

$$\gamma_1 = \frac{\int \left(\frac{T_s - T(\tau_f)}{T_s - T_w}\right)^3 \frac{dF}{dr_0} r_0^3 dr_0}{\int \frac{dF}{dr_0} r_0^3 dr_0} \tag{13}$$

For the SSGF from Zhao et al. (2006), which covers the lower range of drop sizes, γ_1 is generally above 90%, owing to most of the mass being concentrated in the $r_0 = 75$–200 μm range. The SSGF from Ortiz-Suslow et al. (2016) provides an γ_1 that is consistently above 80%, and the SSGF from Troitskaya, Kandaurov, et al. (2018), which covers the widest range of drop sizes, provides an γ_1 that is above 50% at $U_{10} = 40$ m/s and above 80% by $U_{10} = 55$ m/s. Recall only the very smallest drops with radii less than about 100 μm are predicted to evaporate completely at high wind speeds and reenter the sea at nearly the air temperature in this model. Small drops have less enthalpy flux potential than large drops, and their long residence times further limit their contribution to the enthalpy flux. If the volume of the smaller drops ($r_0 < 100$ μm) was predicted by the SSGFs to exceed that of the larger drops, the majority of the ejected sea spray volume would not be expected to reenter near the wet-bulb temperature. However, the SSGFs examined here all reinforce the conclusion that the majority of the sea spray reenters very close to the wet-bulb temperature such that a large fraction of the total possible enthalpy flux potential from sea spray is realized. This first assumption is well-satisfied for $U_{10} \geq 55$ m/s across all SSGFs.

5.2. The Evaporated Mass Is Small

The results from the ensemble also show that the net evaporation is a small fraction of the total ejected mass of sea spray. Figure 4b shows γ_2, which is the fraction of a drop's mass that it is expected to retain upon reentrance, weighted by the total sea spray volume flux from the SSGF

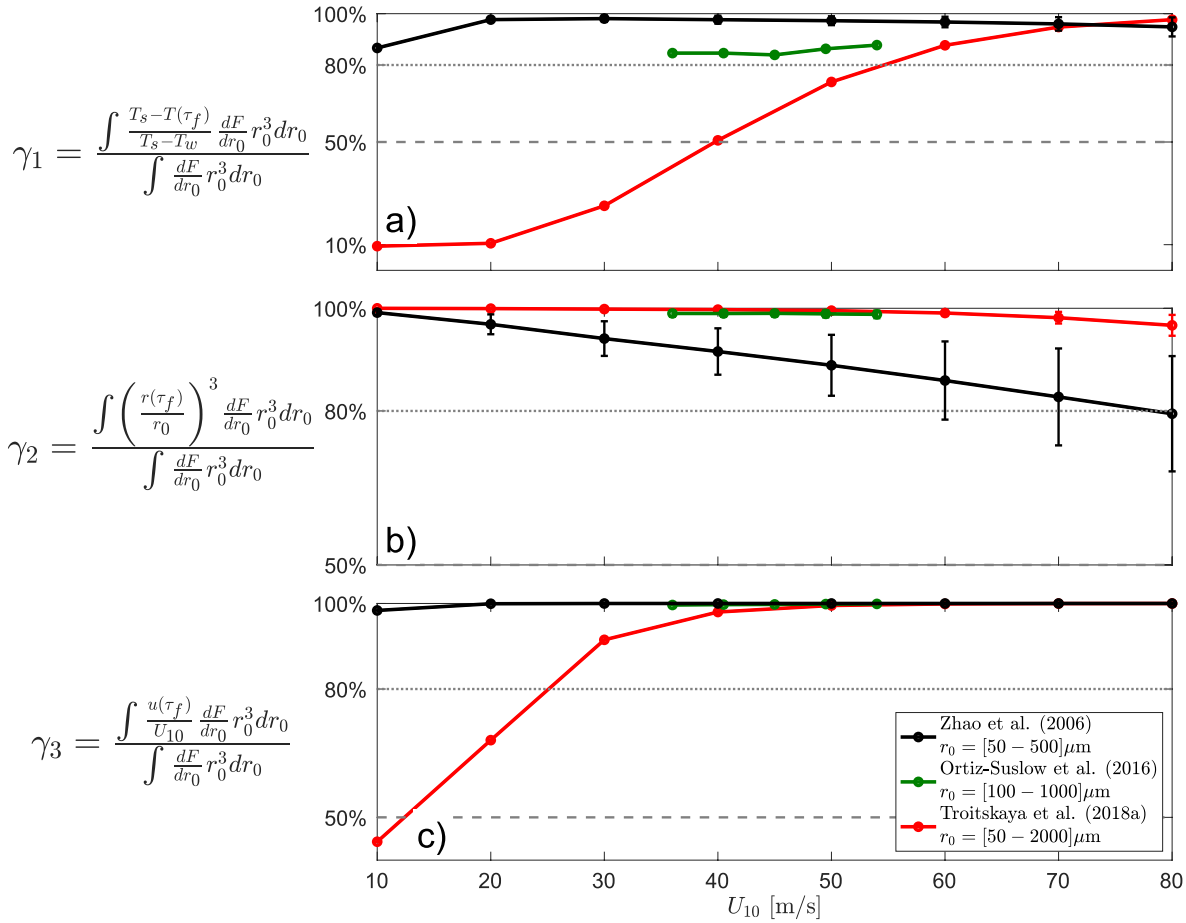

Figure 4. Each filled circle represents the mean of the ensemble, and the whiskers indicate one standard deviation. The top plot shows the fraction of the total spray volume, which reenters at a temperature close to T_w; the average whisker lengths for the black, green, and red curves in this plot are $1.7(10^{-2})$, $6.4(10^{-3})$, and $5.5(10^{-3})$, respectively. The middle plot shows the fraction of the total ejected spray volume that reenters the sea without evaporating; the average whisker lengths for the black, green, and red curves in this plot are $5.5(10^{-2})$, $6.7(10^{-3})$, and $5.3(10^{-3})$, respectively. The bottom plot shows the fraction of the total spray volume, which is accelerated to a velocity U_{10} before reentrance; the average whisker lengths for all three curves in this plot are machine zero. The 50% and 80% levels are indicated with dashed and dotted gray lines, respectively.

$$\gamma_2 = \frac{\int \left(\frac{r(\tau_f)}{r_0}\right)^3 \frac{dF}{dr_0} r_0^3 dr_0}{\int \frac{dF}{dr_0} r_0^3 dr_0}. \tag{14}$$

As expected, more mass evaporates at higher wind speeds as drops remain aloft longer and progress further toward their equilibrium radius r_{eq}. However, the total fraction of reentrant mass is still very large at all wind speeds for all SSGFs. Since small drops will evaporate to their equilibrium radius more quickly than larger drops, the SSGF from Zhao et al. (2006), evaluated for only the smaller drop sizes, exhibits the smallest γ_2 at all wind speeds. The results generally support this second assumption that a very small fraction of the total of ejected mass will evaporate before the drops reenter the sea at all wind speeds.

5.3. Spray Drops Are Accelerated to U_{10}

The velocity time histories, calculated by integrating Equation 8 for all drop sizes, showed that virtually all of the sea spray mass is expected to reenter after having been accelerated to nearly the free stream wind speed U_{10}. Figure 4c shows the sea spray volume flux-weighted fraction γ_3, which compares the speed of the drop at τ_f to U_{10}

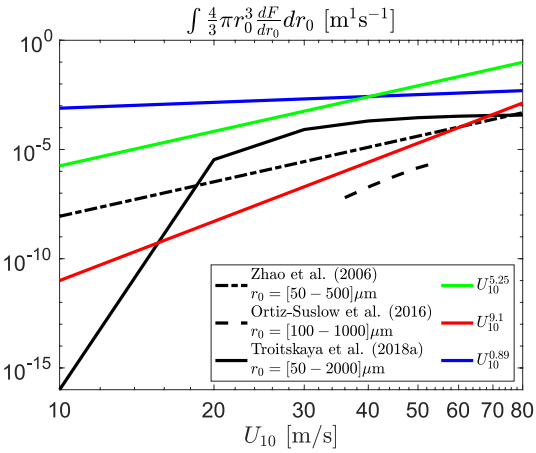

Figure 5. The volume flux of the spray generation functions as a function of U_{10}. Lines with slopes corresponding to the fitted scalings of these volume fluxes demonstrate the sensitivity of the volume flux formulations to U_{10}.

$$\gamma_3 = \frac{\int \left(\frac{u(\tau_f)}{U_{10}}\right)^3 \frac{dF}{dr_0} r_0^3 dr_0}{\int \frac{dF}{dr_0} r_0^3 dr_0}. \quad (15)$$

Recall that the drops are assumed to initially have a negligible horizontal velocity. The results show that this third assumption is well-satisfied for $U_{10} \geq 30$ m/s. As previously mentioned, this calculation technically represents a lower bound on the momentum flux, since the initial radius of the liquid drop is used for the whole integration. Accounting for the fact that the evaporated vapor would readily adjust to the free stream wind speed would slightly enhance γ_3, but would not substantially affect these results since the net evaporated mass is a very small fraction of the total mass of sea spray above $U_{10} = 30$ m/s across all SSGFs considered here.

5.4. Alternate Residence Time Formulations

To help confirm that these results are not overly sensitive to the particular choice of τ_f, the analysis was repeated using two other residence time formulations. The first was a ballistic timescale τ_b where all drops had an initial upward velocity of U_{10} such that $\tau_b = 2U_{10}/g$. This formulation does not change with the size of the drops, and for the range of 10-m wind speeds considered here, τ_b is generally on the order of 10 s. The second residence time formulation keeps the structure of the Andreas (1992) formulation, but the parameterization of the significant wave height H_s from Hsu et al. (2017) is used such that $\tau_{Hsu} = 2H_s/u_f$. This residence time is approximately 66% of the corresponding τ_f for all drop sizes and 10-m wind speeds. The results using these two other residence times (not shown) are very similar to those in Figure 4 with the same threshold at approximately $U_{10} = 55$ m/s and the same behavior in the high wind speed limit, owing largely to the very long time that the drops remain at T_w as shown in Figure 1.

6. Summary

Our results suggest that at extreme wind speeds, the sea spray fluxes are determined by environmental wind and thermodynamic conditions and by the total spray mass flux, but are not sensitive to the shape of the SSGF. The air-sea enthalpy and momentum fluxes are largely determined by U_{10} and the upward spray mass flux. The parameters T_s and T_w will modify the enthalpy flux from sea spray in the hurricane boundary layer. However, if we can consider τ_f from Andreas (1992) to be a good measure of the residence time and the parameter ranges in Table 1 to be representative of typical conditions in the hurricane boundary layer, the variation in T_s and T_w is insufficient in the high wind speed regime to effect a significant change in the air-sea enthalpy flux. The free stream wind speed, U_{10}, is directly proportional to the momentum flux since this wind speed accelerates the lofted spray drops. However, in the high wind speed regime, nearly all of the spray is expected to be accelerated to U_{10} before reentrance. Therefore, the amount of spray produced by the sea surface predominately governs the air-sea enthalpy and momentum fluxes, and the upward sea spray mass flux primarily depends on the wind speed.

All three assumptions used in the mechanistic model are well-satisfied at a 10-m wind speed of around 55 m/s or above for the SSGFs considered here. For typical hurricane spray layer conditions, the microphysical model suggests that above $U_{10} = 55$ m/s, the ratio C_K/C_D becomes independent of wind speed. This agrees well with the results from recent wave tank experiments conducted by Golbraikh and Shtemler (2020) who studied the impact of foam on the surface fluxes. The dependence of the ratio of the exchange coefficients on U_{10} weakens significantly for wind speeds above 50 m/s according to their results.

For a self-similar air-sea transition layer where the ratio of the exchange coefficients no longer depends on the wind speed, the air-sea fluxes could be modeled as functions of the ejected spray volume specified by the SSGF. This means that the relationship between the volume flux of sea spray and U_{10} could be used to simplify the parameterization of sea spray-mediated fluxes in the high wind speed regime. The sea spray volume flux predicted by different SSGFs varies wildly—by many orders of magnitude—among the various SSGFs as shown in Figure 5.

To estimate the sensitivity of the volume fluxes from each SSGF to the 10-m wind speed, each volume flux formulation is written in terms of, or fitted to, a power law function of U_{10}. The SSGF from Zhao et al. (2006) is proportional to $Re_B^{1.5}$ and in their formulation $C_D \propto U_{10}^{0.5}$. Recall that $Re_B = C_D U_{10}^3 \beta/(g\nu_a)$, so the volume flux is proportional to $(U_{10}^{3.5})^{1.5} = U_{10}^{5.25}$. For the next two SSGFs, a least squares regression of the volume flux is used to calculate the coefficients of the power law. The power of U_{10} that results from fitting the volume flux of the SSGF from Ortiz-Suslow et al. (2016) is approximately 9.1 with an R-squared statistic of >0.99. Since the volume flux calculated using the SSGF from Troitskaya, Kandaurov, et al. (2018) is not globally very amenable to this type of fitting, and because this analysis is primarily interested in the high wind speed regime, the least squares fit for this function only considers volume fluxes corresponding to wind speeds above $U_{10} = 30$ m/s. The fitted power of U_{10} for this high wind speed portion of the volume flux is approximately 0.89 with an R-squared statistic of >0.91. These three scalings, shown in Figure 5, underscore that the volume flux could be quite sensitive to changes in the wind speed. Since the SSGF is the element of sea spray-mediated fluxes that, especially in the high wind regime, appears to account for the greatest uncertainty more simulations and experiments of spray generation are needed. Additionally, these should focus on the net spray mass flux rather than on the dependence on drop radii.

Data Availability Statement

The code for the microphysical model used in this study is available at https://doi.org/10.5281/zenodo.5089527.

Acknowledgment
This research was supported by Grant ICER-1854929 from the National Science Foundation.

References

Andreas, E. L. (1989). Thermal and size evolution of sea spray droplets. *Cold Regions Research Engineering Laboratory*, *89*(11).
Andreas, E. L. (1990). Time constants for the evolution of sea spray droplets. *Tellus*, *42B*(5), 481–497. https://doi.org/10.1034/j.1600-0889.1990.t01-3-00007.x
Andreas, E. L. (1992). Sea spray and the turbulent air-sea heat fluxes. *Journal of Geophysical Research*, *97*(3), 11429–11441. https://doi.org/10.1029/92jc00876
Andreas, E. L. (1995). The temperature of evaporating sea spray droplets. *Journal of the Atmospheric Sciences*, *52*(7), 852–862. https://doi.org/10.1175/1520-0469(1995)052<0852:ttoess>2.0.co;2
Andreas, E. L. (2002). A review of the sea spray generation function for the open ocean. *Advances in Fluid Mechanics*, *33*, 1–46.
Andreas, E. L. (2004). Spray stress revisited. *Journal of Physical Oceanography*, *34*, 1429–1440. https://doi.org/10.1175/1520-0485(2004)034<1429:ssr>2.0.co;2
Andreas, E. L. (2005). Approximation formulas for the microphysical properties of saline droplets. *Atmospheric Research*, *75*, 323–345. https://doi.org/10.1016/j.atmosres.2005.02.001
Andreas, E. L., Edson, J. B., Monahan, E. C., Rouault, M. P., & Smith, S. D. (1995). The spray contribution to net evaporation from the sea: A review of recent progress. *Boundary-Layer Meteorology*, *72*, 3–52. https://doi.org/10.1007/bf00712389
Andreas, E. L., & Emanuel, K. (2001). Effects of sea spray on tropical cyclone intensity. *Journal of the Atmospheric Sciences*, *58*(1994), 3741–3751. https://doi.org/10.1175/1520-0469(2001)058<3741:eossot>2.0.co;2
Andreas, E. L., Mahrt, L., & Vickers, D. (2015). An improved bulk air–sea surface flux algorithm, including spray-mediated transfer. *Quarterly Journal of the Royal Meteorological Society*, *141*(687), 642–654. https://doi.org/10.1002/qj.2424
Batchelor, G. (1970). *An introduction to fluid dynamics*. Cambridge university press.
Black, P. G., D'Asaro, E. A., Drennan, W. M., French, J. R., Niiler, P. P., Sanford, T. B., et al. (2007). Air-sea exchange in hurricanes: Synthesis of observations from the coupled boundary layer air-sea transfer experiment. *Bulletin of the American Meteorological Society*, *88*(3), 357–374. https://doi.org/10.1175/BAMS-88-3-357
Clift, R., Grace, J. R., & Weber, M. E. (1978). *Bubbles, drops, and particles* (p. 380). Academic Press.
De Leeuw, G., Andreas, E. L., Anguelova, M. D., Fairall, C., Lewis, E. R., O'Dowd, C., & Schwartz, S. E. (2011). Production flux of sea spray aerosol. *Reviews of Geophysics*, *49*(2), RG2001. https://doi.org/10.1029/2010rg000349
Druzhinin, O. A., Troitskaya, Y. I., & Zilitinkevich, S. S. (2018). The study of momentum, mass, and heat transfer in a droplet-laden turbulent airflow over a waved water surface by direct numerical simulation. *Journal of Geophysical Research: Oceans*, *123*(11), 8346–8365. https://doi.org/10.1029/2018jc014346
Earle, M. D. (1979). Practical determinations of design wave conditions. In *Ocean wave climate* (pp. 39–60). Springer. https://doi.org/10.1007/978-1-4684-3399-9_2
Edson, J., Anquetin, S., Mestayer, P., & Sini, J. (1996). Spray droplet modeling: 2. An interactive Eulerian-Lagrangian model of evaporating spray droplets. *Journal of Geophysical Research*, *101*(C1), 1279–1293. https://doi.org/10.1029/95jc03280
Emanuel, K. (1986). An air-sea interaction theory for tropical cyclones. Part I: Steady-state maintenance. *Journal of the Atmospheric Sciences*, *43*(6), 585–605. https://doi.org/10.1175/1520-0469(1986)043<0585:aasitf>2.0.co;2
Emanuel, K. (1995). Sensitivity of tropical cyclones to surface exchange coefficients and a revised steady-state model incorporating eye dynamics. *Journal of the Atmospheric Sciences*, *52*(22), 3969–3976. https://doi.org/10.1175/1520-0469(1995)052<3969:sotcts>2.0.co;2
Emanuel, K. (2003). A similarity hypothesis for air–sea exchange at extreme wind speeds. *Journal of the Atmospheric Sciences*, *60*(11), 1420–1428. https://doi.org/10.1175/1520-0469(2003)060<1420:ashfae>2.0.co;2
Fairall, C., Banner, M., Peirson, W., Asher, W., & Morison, R. (2009). Investigation of the physical scaling of sea spray spume droplet production. *Journal of Geophysical Research*, *114*(C10), C10001. https://doi.org/10.1029/2008jc004918
Fairall, C., & Larsen, S. E. (1984). Dry deposition, surface production and dynamics of aerosols in the marine boundary layer. *Atmospheric Environment*, *18*(1), 69–77. https://doi.org/10.1016/0004-6981(84)90229-4
Friedlander, S. K. (1977). *Smoke, dust and haze: Fundamentals of aerosol behavior*.

Garg, N., Ng, E. Y. K., & Narasimalu, S. (2018). The effects of sea spray and atmosphere–wave coupling on air–sea exchange during a tropical cyclone. *Atmospheric Chemistry and Physics*, *18*(8), 6001–6021. https://doi.org/10.5194/acp-18-6001-2018

Golbraikh, E., & Shtemler, Y. M. (2020). Momentum and heat transfer across the foam-covered air-sea interface in hurricanes. *Ocean Dynamics*, *70*, 1–10. https://doi.org/10.1007/s10236-020-01360-w

Green, B. W., & Zhang, F. (2014). Sensitivity of tropical cyclone simulations to parametric uncertainties in air–sea fluxes and implications for parameter estimation. *Monthly Weather Review*, *142*(6), 2290–2308. https://doi.org/10.1175/mwr-d-13-00208.1

Holthuijsen, L. H., Powell, M. D., & Pietrzak, J. D. (2012). Wind and waves in extreme hurricanes. *Journal of Geophysical Research*, *117*(9), C09003. https://doi.org/10.1029/2012JC007983

Hsu, S., He, Y., & Shen, H. (2017). Buoy measurements of wind–wave relations during hurricane matthew in 2016. *Journal of Physical Oceanography*, *47*(10), 2603–2609. https://doi.org/10.1175/jpo-d-16-0280.1

Iida, N., Toba, Y., & Chaen, M. (1992). A new expression for the production rate of sea water droplets on the sea surface. *Journal of Oceanography*, *48*(4), 439–460. https://doi.org/10.1007/bf02234020

Jeong, D., Haus, B. K., & Donelan, M. A. (2012). Enthalpy transfer across the air–water interface in high winds including spray, *69*(9), 2733–2748. https://doi.org/10.1175/JAS-D-11-0260.1

Kinsman, B. (1965). *Wind waves prentice-hall*. Inc.

Komori, S., Iwano, K., Takagaki, N., Onishi, R., Kurose, R., Takahashi, K., & Suzuki, N. (2018). Laboratory measurements of heat transfer and drag coefficients at extremely high wind speeds. *Journal of Physical Oceanography*, *48*(4), 959–974. https://doi.org/10.1175/JPO-D-17-0243.1

Lewis, E. R., Lewis, R., Karlstrom, K. E., Lewis, E. R., & Schwartz, S. E. (2004). *Sea Salt Aerosol Production: Mechanisms, Methods, Measurements, and Models* (Vol. 152). American Geophysical Union.

Ma, Y., Davidson, N. E., Xiao, Y., & Bao, J.-W. (2017). Revised parameterization of air–sea exchanges in high winds for operational numerical prediction: Impact on tropical cyclone track, intensity, and rapid intensification. *Weather and Forecasting*, *32*(3), 821–848. https://doi.org/10.1175/waf-d-15-0109.1

Makin, V. K. (2005). A note on the drag of the sea surface at hurricane winds. *Boundary-Layer Meteorology*, *115*(1), 169–176. https://doi.org/10.1007/s10546-004-3647-x

Mehta, S., Ortiz-Suslow, D. G., Smith, A., & Haus, B. (2019). A laboratory investigation of spume generation in high winds for fresh and seawater. *Journal of Geophysical Research: Atmospheres*, *124*(21), 11297–11312. https://doi.org/10.1029/2019jd030928

Mestayer, P., Van Eijk, A., De Leeuw, G., & Tranchant, B. (1996). Numerical simulation of the dynamics of sea spray over the waves. *Journal of Geophysical Research*, *101*(C9), 20771–20797. https://doi.org/10.1029/96jc01425

Monahan, E. C. (1968). Sea spray as a function of low elevation wind speed. *Journal of Geophysical Research*, *73*(4), 1127–1137. https://doi.org/10.1029/jb073i004p01127

Mueller, J. A., & Veron, F. (2014a). Impact of sea spray on air–sea fluxes. Part ii: Feedback effects. *Journal of Physical Oceanography*, *44*(11), 2835–2853. https://doi.org/10.1175/jpo-d-13-0246.1

Mueller, J. A., & Veron, F. (2014b). Impact of sea spray on air–sea fluxes. Part i: Results from stochastic simulations of sea spray drops over the ocean. *Journal of Physical Oceanography*, *44*(11), 2817–2834. https://doi.org/10.1175/jpo-d-13-0245.1

Nayar, K. G., Sharqawy, M. H., Banchik, L. D., & Lienhard, J. H. (2016). Thermophysical properties of seawater: A review and new correlations that include pressure dependence. *Desalination*, *390*, 1–24. https://doi.org/10.1016/j.desal.2016.02.024

Nystrom, R. G., Chen, X., Zhang, F., & Davis, C. A. (2020). Nonlinear impacts of surface exchange coefficient uncertainty on tropical cyclone intensity and air-sea interactions. *Geophysical Research Letters*, *47*(3), e2019GL085783. https://doi.org/10.1029/2019gl085783

O'Dowd, C. D., & De Leeuw, G. (2007). Marine aerosol production: A review of the current knowledge. *Philosophical Transactions of the Royal Society A: Mathematical, Physical & Engineering Sciences*, *365*(1856), 1753–1774.

Ortiz-Suslow, D. G., Haus, B. K., Mehta, S., & Laxague, N. J. (2016). Sea spray generation in very high winds. *Journal of the Atmospheric Sciences*, *73*, 3975–3995. https://doi.org/10.1175/JAS-D-15-0249.1

Peng, T., & Richter, D. (2017). Influence of evaporating droplets in the turbulent marine atmospheric boundary layer. *Boundary-Layer Meteorology*, *165*(3), 497–518. https://doi.org/10.1007/s10546-017-0285-7

Peng, T., & Richter, D. (2019). Sea spray and its feedback effects: Assessing bulk algorithms of air–sea heat fluxes via direct numerical simulations. *Journal of Physical Oceanography*, *49*(6), 1403–1421. https://doi.org/10.1175/jpo-d-18-0193.1

Peng, T., & Richter, D. (2020). Influences of polydisperse sea spray size distributions on model predictions of air-sea heat fluxes. *Journal of Geophysical Research: Atmospheres*, *125*(14), e2019JD032326. https://doi.org/10.1029/2019jd032326

Powell, M. D., Vickery, P. J., & Reinhold, T. A. (2003). Reduced drag coefficient for high wind speeds in tropical cyclones. *Nature*, *422*(March), 279–283. https://doi.org/10.1038/nature01481

Pruppacher, H. R., & Klett, J. D. (1978). *Microphysics of clouds and precipitation*. Springer Netherlands. https://doi.org/10.1007/978-94-009-9905-3_13

Richter, D. H., Dempsey, A. E., & Sullivan, P. P. (2019). Turbulent transport of spray droplets in the vicinity of moving surface waves. *Journal of Physical Oceanography*, *49*(7), 1789–1807. https://doi.org/10.1175/jpo-d-19-0003.1

Richter, D. H., & Stern, D. P. (2014). Evidence of spray-mediated air-sea enthalpy flux within tropical cyclones. *Geophysical Research Letters*, *41*(8), 2997–3003. https://doi.org/10.1002/2014gl059746

Slinn, S., & Slinn, W. (1980). Predictions for particle deposition on natural waters. *Atmospheric Environment*, *14*(9), 1013–1016. https://doi.org/10.1016/0004-6981(80)90032-3

Sroka, S., & Emanuel, K. (2021). A review of parameterizations for enthalpy and momentum fluxes from sea spray in tropical cyclones. *Journal of Physical Oceanography*, *51*(10), 3053-3069. https://doi.org/10.1175/JPO-D-21-0023.1

Toba, Y., & Koga, M. (1986). A parameter describing overall conditions of wave breaking, whitecapping, sea-spray production and wind stress. In *Oceanic whitecaps* (pp. 37–47). Springer. https://doi.org/10.1007/978-94-009-4668-2_4

Toba, Y., Komori, S., Suzuki, Y., & Zhao, D. (2006). Similarity and dissimilarity in air-sea momentum and CO_2 transfers: The nondimensional transfer coefficients in light of windsea Reynolds number. *Atmosphere-ocean interactions*, *2*, 53–82. https://doi.org/10.2495/978-1-85312-929-2/03

Torn, R. D. (2016). Evaluation of atmosphere and ocean initial condition uncertainty and stochastic exchange coefficients on ensemble tropical cyclone intensity forecasts. *Monthly Weather Review*, *144*(9), 3487–3506. https://doi.org/10.1175/mwr-d-16-0108.1

Troitskaya, Y., Druzhinin, O., Kozlov, D., & Zilitinkevich, S. (2018). The "bag breakup" spume droplet generation mechanism at high winds. Part II: Contribution to momentum and enthalpy transfer. *Journal of Physical Oceanography*, *48*(9), 2189–2207. https://doi.org/10.1175/JPO-D-17-0105.1

Troitskaya, Y., Kandaurov, A., Ermakova, O., Kozlov, D., Sergeev, D., & Zilitinkevich, S. (2018). The "bag breakup" spume droplet generation mechanism at high winds. Part I: Spray generation function. *Journal of Physical Oceanography*, *48*(9), 2167–2188. https://doi.org/10.1175/JPO-D-17-0104.1

Van Eijk, A. M., Tranchant, B. S., & Mestayer, P. G. (2001). Seacluse: Numerical simulation of evaporating sea spray droplets. *Journal of Geophysical Research*, *106*(C2), 2573–2588. https://doi.org/10.1029/2000jc000377

Veron, F. (2015). Ocean spray. *Annual Review of Fluid Mechanics*, *47*(1), 507–538. https://doi.org/10.1146/annurev-fluid-010814-014651

Veron, F., Hopkins, C., Harrison, E. L., & Mueller, J. A. (2012). Sea spray spume droplet production in high wind speeds. *Geophysical Research Letters*, *39*(16), L16602. https://doi.org/10.1029/2012GL052603

Villermaux, E., & Bossa, B. (2009). Single-drop fragmentation determines size distribution of raindrops. *Nature Physics*, *5*(9), 697–702. https://doi.org/10.1038/nphys1340

Wilson, B. W. (1965). Numerical prediction of ocean waves in the north Atlantic for december, 1959. *Deutsche Hydrografische Zeitschrift*, *18*(3), 114–130. https://doi.org/10.1007/bf02333333

Zhao, D., & Toba, Y. (2001). Dependence of whitecap coverage on wind and wind-wave properties. *Journal of Oceanography*, *57*(5), 603–616. https://doi.org/10.1023/a:1021215904955

Zhao, D., Toba, Y., Sugioka, K. I., & Komori, S. (2006). New sea spray generation function for spume droplets. *Journal of Geophysical Research*, *111*(2), C02007. https://doi.org/10.1029/2005JC002960

Zhao, D., Toba, Y., Suzuki, Y., & Komori, S. (2003). Effect of wind waves on air'sea gas exchange: Proposal of an overall CO_2 transfer velocity formula as a function of breaking-wave parameter. *Tellus B: Chemical and Physical Meteorology*, *55*(2), 478–487. https://doi.org/10.3402/tellusb.v55i2.16747

Zou, Z., Zhao, D., Tian, J., Liu, B., & Huang, J. (2018). Drag coefficients derived from ocean current and temperature profiles at high wind speeds. *Tellus A: Dynamic Meteorology and Oceanography*, *70*(1), 1–13. https://doi.org/10.1080/16000870.2018.1463805